Astronomy & Astrophysics manuscript no. aa61023-26
July 10, 2026

Letter to the Editor

VLT/SPHERE imaging of the candidate companion of Betelgeuse

M. Montargès[1]⋆, A. Boccaletti[1], O. Flasseur[2], A. de Koter[3], J. Milli[4], P. Kervella[5,1], S. Ridgway[6], E. Bordier[7], E. Lagadec[8], A. K. Dupree[9], F. Backs[10], T. Calderwood[11], and P. Morgan[11]

1 LIRA, Observatoire de Paris, Université PSL, Sorbonne Université, Université Paris Cité, CY Cergy Paris Université, CNRS, 92190 Meudon, France
2 Universite Claude Bernard Lyon 1, Centre de Recherche Astrophysique de Lyon UMR5574, ENS de Lyon, CNRS, Villeurbanne, F-69622, France
3 University of Amsterdam, Anton Pannekoek Institute for Astronomy, 1090 GE, Amsterdam, The Netherlands
4 Univ. Grenoble Alpes, CNRS, IPAG, 38000 Grenoble, France
5 French-Chilean Laboratory for Astronomy, IRL 3386, CNRS and U. de Chile, Casilla 36-D, Santiago, Chile
6 NOIRLab, P.O. Box 26732, Tucson, AZ 85726-6732, USA
7 I.Physikalisches Institut der Universität zu Köln, Zülpicher Str. 77, 50937 Köln, Germany
8 Université Côte dAzur, Observatoire de la Côte dAzur, CNRS, Laboratoire Lagrange, Nice, France
9 Center for Astrophysics-Harvard & Smithsonian, 60 Garden Street, Cambridge, MA 02138, USA
10 Institute of Astronomy, KU Leuven, Celestijnenlaan 200D, 3001 Leuven, Belgium
11 American Association of Variable Star Observers, 185 Alewife Brook Parkway, Suite 410, Cambridge, MA 02138, USA

Received 20 May 2026 / Accepted 19 June 2026

ABSTRACT

Context. Although the binary fraction of massive main-sequence stars is well established, this is much less so the case for red supergiant (RSG) stars due to the primary's brightness as well as its complex and strong surface activity.
Aims. Betelgeuse is the most studied RSG. In 2024, through a reinterpretation of its long secondary period (LSP), a close orbiting stellar companion was suggested to exist, with a maximum elongation in December 2024. Our goal with this work was to search for this secondary component.
Methods. We used extreme adaptive optics direct imaging with the Very Large Telescope SPHERE-ZIMPOL instrument by leveraging the pupil tracking mode of the telescope in angular plus spectral differential imaging (ASDI). Image processing was performed through ASDI PAtch Covariances (PACO ASDI) and principal component analysis (PCA).
Results. The candidate Betelgeuse B was detected at 6.1σ with PACO ASDI and at 5.1σ with PCA in the CntHa filter on December 6, 2024. The separation is 52.32 ± 0.18 mas, and the position angle is $117.12 \pm 0.60°$. Assuming the two stars are coeval, the companion is a 2.6 to 3.1 $M_\odot$ young main-sequence star.
Conclusions. Our observations provide strong evidence that Betelgeuse has a close companion, though formal confirmation that Betelgeuse B is indeed gravitationally bound awaits a second observing epoch. The predicted existence of a companion based on LSP variability and the evidence of the presence of the secondary source reported here identifies LSPs as a potential new avenue for RSG-companion studies, and assessments of their impact on RSG surface and wind structure.

Key words. supergiants – binaries: close – binaries: eclipsing – stars: imaging – circumstellar matter– stars: individual: Betelgeuse

1. Introduction

Red supergiants (RSGs) originate from stars initially 8 to 30 − 35 $M_\odot$ and are the immediate precursors of type-II P/L supernovae (e.g., Smartt 2009; Van Dyk 2025). Massive stars, including the progenitors of RSGs, are thought to all be born as binaries or higher-order multiple systems (Sana et al. 2014). However, the binary fraction of RSGs has been found to be about 20 − 40% (Patrick et al. 2022; Dai et al. 2025). The reason for this difference is likely connected to binary evolution. Such systems in close orbit may interact or even merge before the primary reaches the RSG stage (e.g., de Mink et al. 2013).

Among the two closest RSGs (together with Antares), Betelgeuse (α Ori) is the most scrutinized of its class of stars. The light curve of Betelgeuse is complex and shows semi-regular variations with periods of 2200, 420, 230, and 180 days (Joyce et al. 2020; Jadlovský et al. 2023). The three shortest periods are usually identified as radial pulsation modes (but see Saio et al. 2023), while the nature of the longest period is a matter of debate. Goldberg et al. (2024) and MacLeod et al. (2025) studied the star's light curve in connection with radial velocity variations and astrometry and suggested that this long secondary period (LSP) of 2200 days may indicate the presence of a previously undetected companion that during its transit, once per ∼ 6 years, modulates circumstellar dust in the line of sight. Notably, about 25−30% of all RSGs have been observed to have LSPs (Kiss et al. 2006; Soszyński et al. 2021).

Betelgeuse was reported to be a binary several times in the 20th century, for example, by Karovska et al. (1986), and it appears in several binary catalogs (Proust et al. 1981; Wycoff et al. 2006). So far these claims lack independent confirmation.

Goldberg et al. (2025) and O'Grady et al. (2025) respectively reported non-detection at the maximum elongation epoch

⋆ Corresponding author: miguel.montarges@obspm.fr

with far-ultraviolet Hubble Space Telescope (HST) and Chandra X-ray observations. Howell et al. (2025) employed the suggested orbital properties of Goldberg et al. (2024) and MacLeod et al. (2025) to search for a companion using the 'Alopeke speckle imager at the Gemini North telescope in Hawai'i. They reported a tentative detection at the predicted maximum elongation of 52 mas in December 2024, but only at a 1.5σ level. Subsequently, Dupree et al. (2026) reported on the effect of the companion on the circumstellar material and the chromosphere through HST spectrometry.

Here, we present Very Large Telescope (VLT) observations of Betelgeuse with the Spectro-Polarimetric High-contrast Exoplanet REsearch (SPHERE) instrument at the epoch of the 2024 maximum elongation of the hypothetical companion. The observations and their reduction are discussed in Sect. 2. The data analysis, leading to a 6.1σ detection of the candidate companion, and mapping of dust clouds in the circumstellar environment (CSE) are the topics of Sect. 3. Our findings are discussed in Sect. 4. Concluding remarks are made in the final section.

2. Observations and data reduction

Betelgeuse was observed with SPHERE (Beuzit et al. 2019) on the nights of December 3 and 6, 2024, using the Zurich IMaging POLarimeter (ZIMPOL; Schmid et al. 2018), which operates in the visible domain. We used two observation strategies: polarized imaging to obtain the Q and U Stokes maps and angular plus spectral differential imaging (ASDI) in intensity. In both cases, no coronograph was used. The log of the observations is available in Table A.1.

Data were reduced through the High Contrast Data Centre (HC-DC[1]; Delorme et al. 2017). Processing of the ZIMPOL polarized data is detailed in Montargès et al. (2023). The Q and U Stokes maps allowed the degree of linear polarization (DoLP) to be derived. For the intensity images, HC-DC provided us with a temporal sequence of frames obtained in pupil tracking, where most aberrations are fixed and any astrophysical signal is rotating. In Sect. 3, we present two algorithms to disentangle aberrations and the astrophysical signal.

We relied on photometry obtained by observers from the American Association of Variable Star Observers (AAVSO[2]). In particular, we used data obtained by Tom Calderwood (CTOA) and Pam Morgan-McKee (MPFA) in the V filter on December 1 and 4, 2024, closest in time to our SPHERE imaging. The error bars on these measurements are estimated to 0.01 mag.

3. Data analysis

3.1. PACO ASDI: Detection of candidate Betelgeuse B

The temporal sequence of total intensity frames provided by the HC-DC were processed with the angular plus spectral differential imaging PAtch COvariances algorithm (PACO ASDI; Flasseur et al. 2020a,b and App. C, see Fig. 1) and through principal component analysis (PCA; Soummer et al. 2012; Amara & Quanz 2012, see Fig. D.1). The two techniques give consistent results: No other secondary component is detected in the NHa filter (narrow-Hα, centered at 656.34 nm with a width of 0.97 nm). However, a secondary source appears in the CntHa filter (continuum near Hα, centered at 644.9 nm with a width of 4.1 nm). The contrast estimation is shown in Fig. C.1.

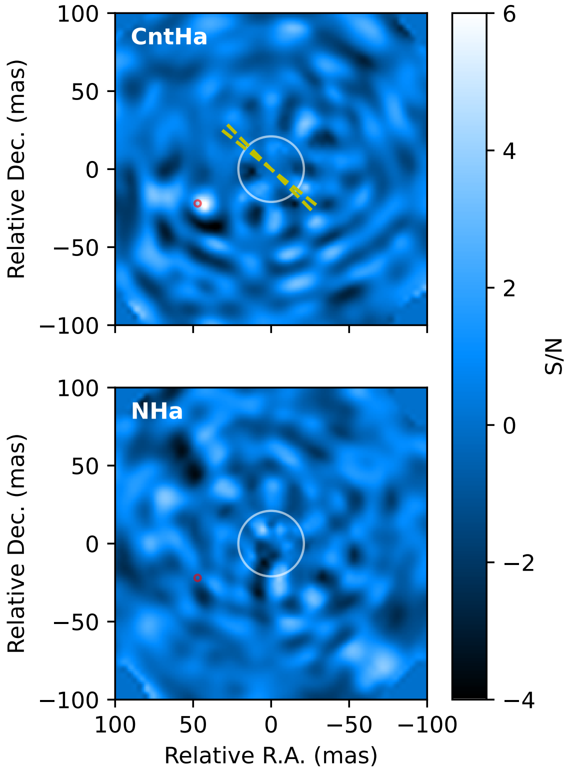

Fig. 1: PACO ASDI analysis of the Betelgeuse observations with ZIMPOL on December 6, 2024. The white circle shows the position and infrared angular size (from Montargès et al. 2021) of the primary (subtracted during the analysis); the red circle corresponds to the candidate companion detection by Howell et al. (2025) on December 9, 2024. Dashed yellow lines represent the cone of uncertainty for the presumed rotation axis of the primary (Kervella et al. 2018). *Top:* CntHa filter. *Bottom:* NHa filter.

Here, we focus on the PACO ASDI analysis, which is optimized for detecting point sources. The PCA analysis is presented in Appendix D. The secondary source characteristics retrieved from PACO in the CntHa filter are the following:

$$\begin{aligned} \rho &= 52.32 \pm 0.18 \text{ mas}, \\ \text{PA} &= 117.12 \pm 0.60^\circ, \\ F_\text{B}/F_\text{A} &= (8.24 \pm 1.04) \times 10^{-4}, \\ \text{S/N} &= 6.1, \end{aligned}$$

with ρ as the projected separation, PA as the corresponding position angle (with 0° toward north and 90° toward east), and F_B/F_A as the contrast ratio. The reported uncertainties encompass both the PACO ASDI extraction uncertainty, driven by the high-contrast of the observations, and additional sources of systematic instrumental errors. For the evaluation of the latter, we followed a procedure similar to that described in Chomez et al. (2023, Sects. 4.3.1 and 4.3.2). All sources of error were then added quadratically to obtain the reported total astrophotometric error budget. The retrieved source characteristics are in good agreement with the 1.5σ detection of Howell et al. (2025). We thus confirm their analysis and refer to this secondary source as Betelgeuse B. Howell et al. used two imaging epochs and concluded that the probability of the candidate companion being a background or foreground star is negligible. Still, until the candidate Betelgeuse B is observed on the other side of the

[1] https://hc-dc.cnrs.fr/
[2] https://www.aavso.org

primary after half an orbital period, we conservatively refer to it as a "candidate."

3.2. Degree of linear polarization: The signature of dust

Figure B.1 shows the DoLP measured by ZIMPOL in the inner environment of Betelgeuse on the December 3, 2024. Patches of brighter DoLP are seen at a distance of ~ 1 to about 4.5 $R_\star$, beyond which the image sensitivity drops steeply. Following previous DoLP-imaging from Kervella et al. (2016), we identify the signal as light scattering on dust grains. Cannon et al. (2021) and Montargès et al. (2023) have shown that the efficiency of dust scattering depends on various dust characteristics, such as composition and grain size distribution, as well as on the amount of dust and its spatial distribution relative to the star. The polarized signal is most efficiently produced by dust that is in the plane of the sky and through the center of Betelgeuse A, with the preferred scattering angle being 90°.

4. Discussion

4.1. Agreement with the published orbital solution

Relying only on one epoch of observation does not allow us to assert whether the orbital solutions from Goldberg et al. (2024) and MacLeod et al. (2025) are accurate. Though we detected the candidate Betelgeuse B on December 6, 2024, we cannot claim that it is precisely at or near maximum elongation as assumed by the two previous studies. However, the projected separation can serve as a lower limit for the semimajor axis: $8.80^{+1.41}_{-0.79}$ au, for a distance of 168^{+27}_{-15} pc from Joyce et al. (2020). For their primary mass of 16.5 − 19 M$_\odot$, this leads to an orbital period of at least $(5.9 - 5.5)^{+1.5}_{-0.7}$ yr. This is consistent with the orbital periods of 5.94 and 5.78 yr derived by Goldberg et al. (2024) and MacLeod et al. (2025).

These period estimates are in line with the LSP of 2200 d (or 6.0 yr). However, we note that if Betelgeuse is considerably more distant than 168 pc, the LSP may no longer match the orbital period. The distance determination of Betelgeuse has been problematic for decades: The optical parallax is constrained within the star's apparent disk, and surface convection causes photocenter displacements (Chiavassa et al. 2022). To address these issues, Harper et al. (2017) used a radio parallax, which is anticipated to be less sensitive to convection. With their distance estimate of 222^{+48}_{-34} pc, the minimum semimajor axis of the orbit of Betelgeuse B would be $11.6^{+2.51}_{-1.78}$ au, leading to a minimum orbital period of $(8.7 - 8.2)^{+3.1}_{-1.7}$ yr. This does not match the LSP as well. We conclude that the asteroseismology-based distance of Joyce et al. (2020) of 168^{+27}_{-15} pc better fits the hypothesis that LSP variability is related to binary motion.

4.2. Compatibility with the inferred rotation axis

The PA of the rotation axis has been estimated at 48.0 ± 3.5° by Kervella et al. (2018), implying the equatorial plane is at 138°. This is offset by more than 20° with respect to the PA of Betelgeuse B in our images. The observations can quite easily be reconciled with an aligned rotation axis and orbital plane orientation if the rotation axis of Betelgeuse A is not within the plane of the sky, as suggested by earlier HST observations (Uitenbroek et al. 1998), or if the companion is not exactly observed at maximum elongation and the orbit possesses a modest inclination. We point to Ma et al. (2024) for an alternative interpretation of the photospheric velocity field other than rotation.

4.3. On the nature of candidate Betelgeuse B

We used the contrast between the two components to estimate the spectral flux density of Betelgeuse B in the CntHa filter. To obtain the corresponding value for Betelgeuse A, we used a RSG Phoenix model (Lançon et al. 2007) with an effective temperature of 3700 K and effective gravity $\log g$ [cm s^{-2}] = 0.0 (Montargès et al. 2021) and scaled the AAVSO photometry, correcting for extinction using the expression from Cardelli et al. (1989) with A_V = 0.65 and R_V = 4.2 (Montargès et al. 2021). The angular diameter was adjusted to $40.0^{+0.2}_{-0.5}$ mas to match the AAVSO photometry. The adopted distance was 168^{+27}_{-15} pc (Joyce et al. 2020). This yielded $(4.27 \pm 0.07) \times 10^{-8}$ and $(3.44 \pm 0.44) \times 10^{-11}$ W m^{-2} μm^{-1} for components A and B, respectively. The error bars are dominated by the distance uncertainty.

We investigated the nature of Betelgeuse B by assuming the system components are coeval. For Betelgeuse A, Joyce et al. (2020) estimate an initial mass in the range of 18 − 21 M$_\odot$ and an age since arrival on the main sequence (MS) of ~ 8 − 10.5 Myr. We used MIST pre-MS evolutionary tracks of Dotter (2016) and Choi et al. (2016) to first assess that the lifetime of the pre-MS stage of Betelgeuse A is negligibly short (see also, Backs et al. 2024). We then took spectral energy distributions (SEDs) from the Phoenix library (Husser et al. 2013) and attributed to them properties representing stars on a pre-MS isochrone of 8 − 10.5 Myr and matched them to our flux estimation in the CntHa filter (see Table E.1). The result is shown in Fig. 2 and conveys that the companion is best matched by a 2.6 − 3.1 M$_\odot$ star of spectral type B8.5V−B9.5V that has just arrived on the MS (see Fig. E.1). This mass range is probably broader due to the inhomogeneous circumstellar dust extinction that cannot be estimated with our data. Together with the inclination of the system discussed in Sect. 4.2, this makes our estimates compatible with the mass prediction of Goldberg et al. (2024).

Young MS stars (and part of the weak T Tauri star population) have a depleted or dispersed circumstellar accretion disk, and hence Hα emission, if any, is the result of chromospheric activity only (e.g., Barrado y Navascués & Martín 2003). Therefore, the non-detection of Hα emission in the NHa filter, the absence of far ultraviolet detection from HST (Goldberg et al. 2025), and the lack of X-ray signal in the Chandra observations (O'Grady et al. 2025) are consistent with Betelgeuse B being a young MS star instead of a pre-MS star.

4.4. The mechanism of the LSP-amplitude modulation

The work of Goldberg et al. (2024) and MacLeod et al. (2025) relies on the assumption that the LSP is due to orbital motion; that is, the specific mechanism by which the candidate companion causes the visible light variations is not relevant for their conclusions. One hypothesis that can be easily checked is whether circumstellar dust sublimation by the companion is sufficient to generate the LSP in magnitude. Imaging reveals that though the wind of Betelgeuse A is extremely "clumpy," ample dust is present at the location of the companion (see our Fig. B.1 and, e.g., Kervella et al. 2011, 2016; Montargès et al. 2021). Assuming dust particles to be gray absorbers and to sublimate at T_d ~ 1500 K, we estimate that dust is destroyed up to about 0.3 au (or 2.0 mas) from the companion, adopting the parameters for a 3.1 M$_\odot$ star. Assuming the candidate compan-

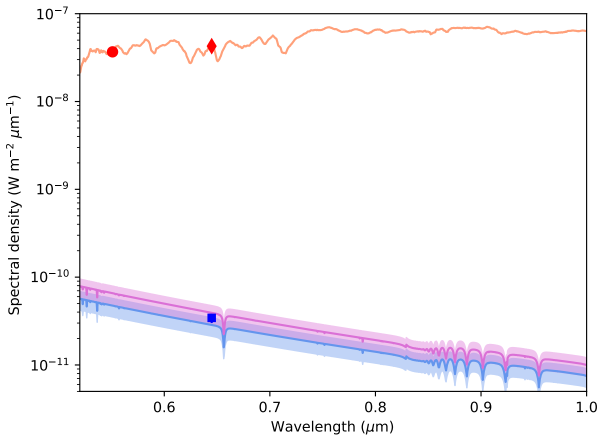

Fig. 2: SED of the Betelgeuse system. The red circular marker corresponds to the AAVSO photometry of Betelgeuse A in the V band. The light orange curve is a Phoenix model matching the photometry. The red diamond is the derived photometry of Betelgeuse A in the ZIMPOL CntHa filter. The blue square is the derived photometry of Betelgeuse B. The violet (resp. light blue) curve is a Phoenix model for a 3.1 $M_{\odot}$ (resp. 2.6 $M_{\odot}$) pre-MS star (see Table E.1), with the shaded areas representing the uncertainty on the distance to the system.

ion transits in the equatorial plane and is able to clear out all dust along its path and along the line of sight, it provides an extinction free view of ∼ 12.0% of the total apparent disk of Betelgeuse A, with 42.6 mas being the photospheric diameter of Betelgeuse A (Montargès et al. 2021). Depending on the line-of-sight optical extinction of the wind, at best this produces a modulation of ∼ 0.1 mag. This is less than the ∼ 0.5 mag modulation of the LSP (Goldberg et al. 2024). We propose that the LSP is mainly created through dynamical effects, as already proposed by Goldberg et al. (2024) and MacLeod et al. (2025) and discussed by Decin et al. (2025) for lower-mass primary stars.

In the DoLP map at maximum elongation (Fig. B.1), obtained a few days before the ASDI detection, the companion is located in a bright patch. Bright patches indicate the presence of dust in the plane of the sky going through Betelgeuse A. Using the estimate of the dust evaporation zone around the companion obtained above, the companion's impact on dust destruction is below the angular resolution limit.

5. Conclusions

We have presented VLT/SPHERE-ZIMPOL imaging of Betelgeuse in relation to a search for a companion tentatively (at 1.5σ) identified by Howell et al. (2025). We confirm the presence of this companion at the 6.1σ level. At the time of our observations, it was located at a projected distance from Betelgeuse A of 52.32±0.18 mas or $8.80^{+1.41}_{-0.79}$ au, adopting a distance of 168^{+27}_{-15} pc (Joyce et al. 2020). For a primary mass of 16.5 – 19 $M_{\odot}$, we find an orbital period of at least $(5.9 - 5.5)^{+1.5}_{-0.7}$ yr. This agrees, within uncertainties, with the orbital analysis by Goldberg et al. (2024) and MacLeod et al. (2025). Our orbital period constraints align with Betelgeuse's LSP period of ∼2200 d (∼ 6.02 yr) and are in line with the hypothesis that the LSP variability may be linked to orbital motion.

Howell et al. (2025) estimate that the probability Betelgeuse B is a line-of-sight coincidence rather than a gravitationally bound partner star is negligible. Still, to definitively confirm it as a true companion, Betelgeuse B should be observed on the opposite side of the primary after half an orbital period. Even more observations will then be needed to firmly constrain the orbital solution. This will aid in further investigating the nature, evolutionary past, and future fate of the Betelgeuse system. It is also necessary to cross-check the RSG population showing LSP variability against other binary indicators, such as radial velocity variability, far-ultraviolet excess, and blue-star features (see, e.g., Dai et al. 2025), in order to assess whether this type of photometric variability indeed points to binarity.

Data availability

The VLT/SPHERE raw and processed data are readily available on the ESO archive. AAVSO observations are publicly available.

Acknowledgements. Based on observations collected at the European Southern Observatory under ESO programme 114.28H9.001. This work has made use of the High Contrast Data Centre, jointly operated by OSUG/IPAG (Grenoble), PYTHEAS/LAM/CeSAM (Marseille), OCA/Lagrange (Nice), Observatoire de Paris/LIRA (Paris), and Observatoire de Lyon/CRAL, and supported by a grant from Labex OSUG@2020 (Investissements d'avenir ANR10 LABX56). We thank the anonymous referee for useful comments that improved the quality of the paper. EB acknowledges support by the CRC 1601 (SFB1601 sub project A3) funded by the DFG german research fundation - grant number 500700252. The research leading to these results has received funding from the European Research Council (ERC) under the European Union's Horizon 2020 research and innovation program (project UniverScale, grant agreement 951549).

References

Amara, A. & Quanz, S. P. 2012, MNRAS, 427, 948
Backs, F., Brands, S. A., Ramírez-Tannus, M. C., et al. 2024, A&A, 690, A113
Barrado y Navascués, D. & Martín, E. L. 2003, AJ, 126, 2997
Beuzit, J.-L., Vigan, A., Mouillet, D., et al. 2019, A&A, 631, A155
Cannon, E., Montargès, M., de Koter, A., et al. 2021, MNRAS, 502, 369
Cardelli, J. A., Clayton, G. C., & Mathis, J. S. 1989, ApJ, 345, 245
Chiavassa, A., Kudritzki, R., Davies, B., Freytag, B., & de Mink, S. E. 2022, A&A, 661, L1
Choi, J., Dotter, A., Conroy, C., et al. 2016, ApJ, 823, 102
Chomez, E., Lagrange, A.-M., Delorme, P., et al. 2023, A&A, 675, A205
Dai, M., Wang, S., & Jiang, B. 2025, MNRAS, 539, 1220
de Mink, S. E., Langer, N., Izzard, R. G., Sana, H., & de Koter, A. 2013, ApJ, 764, 166
Decin, L., Vermeulen, O., Esseldeurs, M., et al. 2025, A&A, 703, L23
Delorme, P., Meunier, N., Albert, D., et al. 2017, in SF2A-2017 Proc. Annu. Meet. Fr. Soc. Astron. Astrophys. (eprint: arXiv:1712.06948: arXiv)
Dotter, A. 2016, ApJS, 222, 8
Dupree, A. K., Cristofari, P. I., MacLeod, M., & Kravchenko, K. 2026, ApJ, 998, 50
Flasseur, O., Denis, L., Thiébaut, É., & Langlois, M. 2020a, A&A, 637, A9
Flasseur, O., Denis, L., Thiébaut, É., & Langlois, M. 2020b, A&A, 634, A2
Goldberg, J. A., Joyce, M., & Molnár, L. 2024, ApJ, 977, 35
Goldberg, J. A., O'Grady, A. J. G., Joyce, M., et al. 2025, ApJ, 994, 101
Harper, G. M., Brown, A., Guinan, E. F., et al. 2017, AJ, 154, 11
Howell, S. B., Ciardi, D. R., Clark, C. A., et al. 2025, ApJ, 988, L47
Husser, T.-O., Wende-von Berg, S., Dreizler, S., et al. 2013, A&A, 553, A6
Jadlovský, D., Krtička, J., Paunzen, E., & Štefl, V. 2023, NewA, 99, 101962
Joyce, M., Leung, S.-C., Molnár, L., et al. 2020, ApJ, 902, 63
Karovska, M., Nisenson, P., & Noyes, R. 1986, ApJ, 308, 260
Kervella, P., Decin, L., Richards, A. M. S., et al. 2018, A&A, 609, A67
Kervella, P., Lagadec, E., Montargès, M., et al. 2016, A&A, 585, A28
Kervella, P., Perrin, G., Chiavassa, A., et al. 2011, A&A, 531, A117
Kiss, L. L., Szabó, Gy. M., & Bedding, T. R. 2006, MNRAS, 372, 1721
Lançon, A., Hauschildt, P. H., Ladjal, D., & Mouhcine, M. 2007, A&A, 468, 205
Ma, J.-Z., Chiavassa, A., de Mink, S. E., et al. 2024, ApJ, 962, L36
MacLeod, M., Blunt, S., De Rosa, R. J., et al. 2025, ApJ, 978, 50
Montargès, M., Cannon, E., de Koter, A., et al. 2023, A&A, 671, A96
Montargès, M., Cannon, E., Lagadec, E., et al. 2021, Nature, 594, 365
O'Grady, A. J. G., O'Connor, B., Goldberg, J. A., et al. 2025, ApJ, 992, 107
Patrick, L. R., Thilker, D., Lennon, D. J., et al. 2022, MNRAS, 513, 5847
Proust, D., Ochsenbein, F., & Pettersen, B. R. 1981, A&AS, 44, 179
Saio, H., Nandal, D., Meynet, G., & Ekström, S. 2023, MNRAS, 526, 2765
Sana, H., Le Bouquin, J.-B., Lacour, S., et al. 2014, ApJS, 215, 15
Schmid, H. M., Bazzon, A., Roelfsema, R., et al. 2018, A&A, 619, A9
Smartt, S. J. 2009, ARA&A, 47, 63
Soszyński, I., Olechowska, A., Ratajczak, M., et al. 2021, ApJ, 911, L22
Soummer, R., Pueyo, L., & Larkin, J. 2012, ApJ, 755, L28
Uitenbroek, H., Dupree, A. K., & Gilliland, R. L. 1998, AJ, 116, 2501
Van Dyk, S. D. 2025, Galax, 13, 33
Wycoff, G. L., Mason, B. D., & Urban, S. E. 2006, AJ, 132, 50

Appendix A: Observation log

Table A.1: Observation log.

Object	Date	Time (UT)	Mode	ND	Filter arm 1	Filter arm 2	Seeing (arcsec)	DIT (s)	NDIT	# frames	Δ para. ang. (°)
Betelgeuse	2024-12-03	04:47	P1	ND2	V	N_I	0.51	0.1	22	-	-
Betelgeuse		04:57	P1	ND4	V	N_I	0.51	3.0	2	-	-
Rigel		05:34	P1	ND4	V	N_I	0.56	3.0	4	-	-
Betelgeuse	2024-12-06	04:37	Total Intensity PT	ND1	CntHα	N_Hα	0.59	1.0	20	40	-0.27
Betelgeuse		04:39	Total Intensity PT	ND2	CntHα	N_Hα	0.7	1.0	20	1380	-11.22
Betelgeuse		05:08	Total Intensity PT	ND2	CntHα	N_Hα	0.58	1.0	20	1380	-12.31
Betelgeuse		05:37	Total Intensity PT	ND2	CntHα	N_Hα	0.49	1.0	20	1380	-12.2
Betelgeuse		06:06	Total Intensity PT	ND2	CntHα	N_Hα	0.46	1.0	20	1380	-11.03
Rigel		06:42	Total Intensity PT	ND2	CntHα	N_Hα	0.57	1.0	20	900	-3.42

Notes. P1 is one of the two polarization modes of ZIMPOL. PT stands for pupil tracking. ND refers to the neutral densities. DIT is the detector integration time; NDIT is the number of integrations for each frames, and # frames gives the number of frames. Δ para. ang. is the parallactic angle exploration for the ASDI observations. The characteristics of the SPHERE filters are available at https://www.eso.org/sci/facilities/paranal/instruments/sphere/inst/filters.html.

Appendix B: SPHERE-ZIMPOL DoLP map

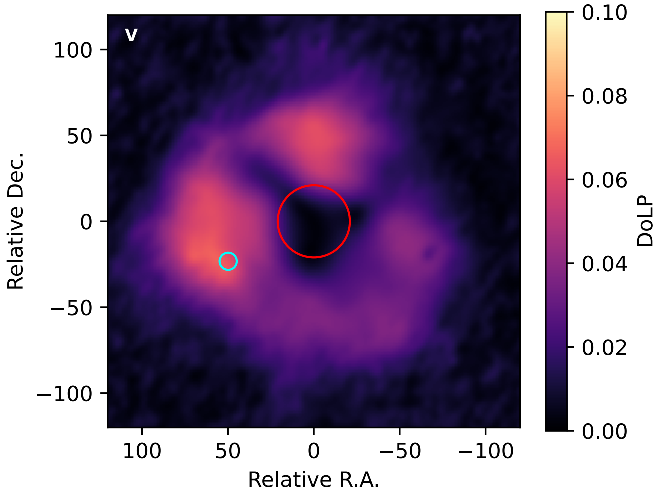

Fig. B.1: Degree of linear polarization, DoLP, observed with VLT/SPHERE-ZIMPOL around Betelgeuse on December 3, 2024. The red circle shows the position and infrared angular size (from Montargès et al. 2021) of the primary, and the cyan circle corresponds to the candidate companion detection by Howell et al. (2025).

Appendix C: PACO ASDI

PACO ASDI (Flasseur et al. 2020a,b) builds a statistical model of the spatial and spectral structures (i.e., correlations) of the nuisance corrupting high contrast observations (i.e., speckles and stochastic noises). The parameters of the underlying multivariate Gaussian model (i.e., temporal mean fluctuations, covariances, temporal and spectral weighting) are estimated locally, at a scale of patches of a few tens of pixels. Given that the 2024 observations were obtained without a coronagraphic mask and that the primary component is partially resolved, we adopt slight modifications to the original algorithm. We construct a synthetic off-axis point spread function (PSF) with a brightness similar to that of the primary component and use it as the off-axis PSF template for the detection. We also manually fix the patch size (5 pixels of radius), instead of using the default criterion of twice the PSF full width at half maximum, as this would otherwise lead to excessively large patches and prevent covariance estimation by making the model too complex. These choices are mainly practical and only slightly affect the detection signal-to-noise ratio (S/N) and the estimated astrometry and photometry, provided that covariance estimation remains feasible. After detection, the source parameters (astrometry and photometry) are refined through a local optimization performed jointly with the nuisance parameters. This strategy mitigates biases caused by the partial absorption of the source signal into the nuisance model, i.e., the self-subtraction effect.

Appendix D: Principal component analysis

We applied a PCA on the ZIMPOL data for both filters varying the number of truncated modes from 50 to 1000 (out of 5450 frames of 5520 in total). The candidate companion Betelgeuse B, is detected (S/N $\approx$ 5) as the brightest feature in CntHa for truncation of 200, 500, and 1000, while it remains undetected in the narrow band filter NHa. We used the forward modeling framework to estimate the astro-photometry of the object assuming it is a point source. The point source data cube model undergoes the same projection and truncation as the data in order to estimate for the self-subtraction in an aperture of 8 pixels (28 mas) in radius. The position is further optimized by minimizing the forward model image in the data. We obtain an astrometric solution that is identical for the three cases, and consistent with PACO estimates within error bars: ρ = 53.23 mas and PA = 120.18°. The corresponding detection map is shown on Fig. D.1. As for the photometry, a qualitative estimation of the error bar is obtained from the dispersion of the contrast values obtained for the three truncations. We derived a contrast value of $(1.76 \pm 0.29) \times 10^{-4}$, which is significantly lower than the estimation of PACO. However, we consider it as little reliable given the level of the self subtraction, since PCA needs a large truncation for the source to be detected, and also because of the size of integration aperture, as well as the potential contamination of the environment of the primary which may bias PCA.

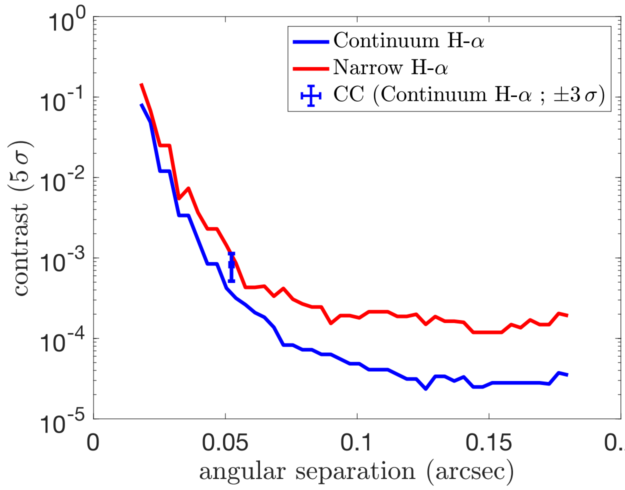

Fig. C.1: Estimated 5σ contrast as a function of angular separation with the PACO ASDI analysis of our observations, both in the CntHA (blue) and NHa (red) filters. The blue marker shows the CntHa detection.

Appendix E: Age of candidate Betelgeuse B

Table E.1: Pre-main-sequence stellar properties for a 2.6 and 3.1 $M_\odot$ star on the 8 – 10.5 Myr isochrone from Dotter (2016) and Choi et al. (2016).

Pre-main-sequence model	2.6 $M_\odot$	3.1 $M_\odot$
Effective temperature (K)	11 200	12 000
L ($L_\odot$)	47.3	92.2
R ($R_\odot$)	1.83	2.01

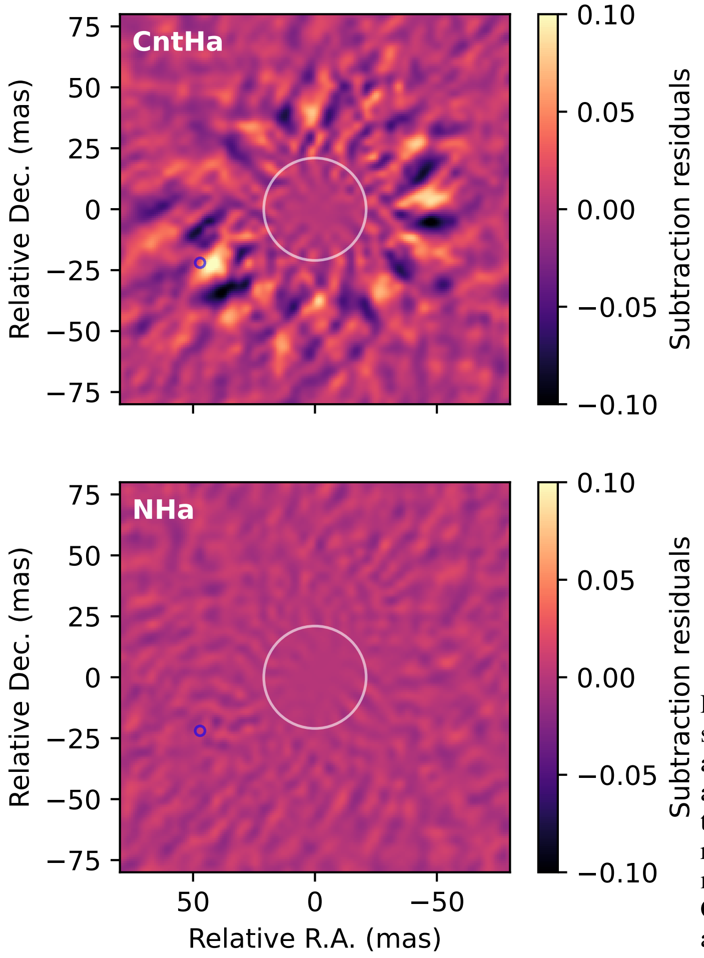

Fig. D.1: Output from the PCA of the ADI observations of Betelgeuse with ZIMPOL on December 6, 2024. The maps show the residuals after subtraction of a low-rank model of the nuisance. The white circle shows the position and infrared angular size (from Montargès et al. 2021) of the primary, and the blue circle corresponds to the companion detection by Howell et al. (2025). *Top:* CntHa filter. *Bottom:* NHa filter.

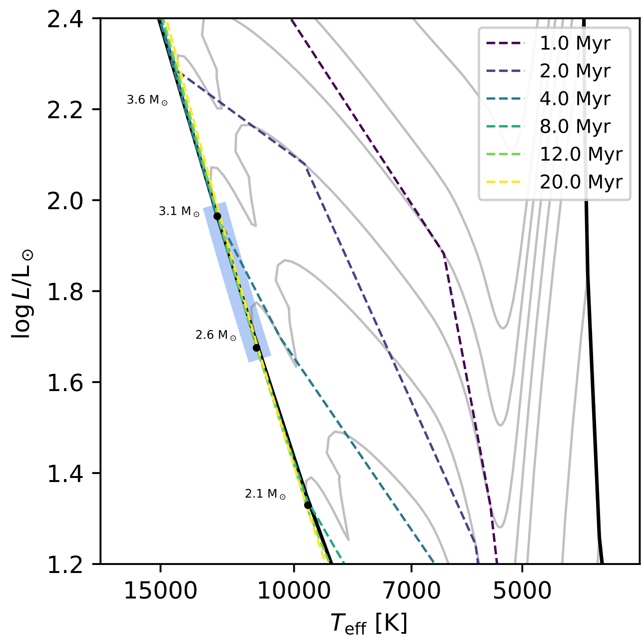

Fig. E.1: Pre-main-sequence tracks for stars with zero-age main-sequence masses of 2.1, 2.6, 3.1 and 3.6 $M_\odot$ from Dotter (2016) and Choi et al. (2016). Assuming coevality of the stars and adopting an age of 8 – 10.5 Myr for Betelgeuse A, we find that the companion has just arrived on the main-sequence. The blue rectangle overlaying the light blue 8 Myr isochrone brackets the mass range that reproduces the observed continuum flux in the CntHa filter, within its uncertainties, adopting Phoenix model atmospheres (Husser et al. 2013) for the star's SED. This mass range is from 2.6–3.1 $M_\odot$. Stellar properties for the boundaries of this range are given in Table E.1.